

The Mass Function of Main Sequence Stars in NGC 6397 from Near IR and Optical High Resolution HST Observations¹

Guido De Marchi, Francesco Paresce, and Luigi Pulone²

European Southern Observatory, Karl-Schwarzschild Strasse 2, D-85748 Garching, Germany
demarchi@eso.org, fparesce@eso.org, lpulone@eso.org

Accepted for publication in “The Astrophysical Journal”

ABSTRACT

We have investigated the properties of the stellar mass function in the globular cluster NGC 6397 through the use of a large set of HST observations. The latter include existing WFPC 2 images in the V and I bands, obtained at $\sim 4.5'$ and $10'$ radial distances, as well as a series of deep images in the J and H bands obtained with the NIC 2 and NIC 3 cameras of the NICMOS instrument pointed, respectively, to regions located $\sim 4.5'$ and $\sim 3.2'$ from the center. These observations span the region from ~ 1 to ~ 3 times the cluster’s half-light radius ($r_{\text{hl}} \simeq 3'$), and have been subjected to the same, homogeneous data processing so as to guarantee that the ensuing results could be directly compared to one another. We have built color–magnitude diagrams that we use to measure the luminosity function of main sequence stars extending from just below the turn-off all the way down to the Hydrogen burning limit. All luminosity functions derived in this way show the same, consistent behavior in that they all increase with decreasing luminosity up to a peak

¹Based on observations with the NASA/ESA *Hubble Space Telescope*, obtained at the Space Telescope Science Institute, which is operated by AURA, Inc., under NASA contract NAS5-26555

²On leave from the Osservatorio Astronomico di Roma, Rome, Italy

at $M_I \simeq 8.5$ or $M_H \simeq 7$ and then drop precipitously well before photometric incompleteness becomes significant. Within the observational uncertainties, at $M_I \simeq 12$ or $M_H \simeq 10.5$ ($\sim 0.09 M_\odot$) the luminosity functions are compatible with zero. The direct comparison of our NIC 2 field with previous WFPC 2 observations of the same area shows that down to $M_H \simeq 11$ there are no more faint, red stars than those already detected by the WFPC 2, thus excluding a significant population of faint, low-mass stars at the bottom of the main sequence. By applying the best available mass–luminosity relation appropriate to the metallicity of NGC 6397 and consistent with our color–magnitude diagrams to both the optical and IR data, we obtain a mass function that shows a break in slope at $\sim 0.3 M_\odot$. No single exponent power-law distribution is compatible with these data, regardless of the value of the exponent. We find that a dynamical model of the cluster can simultaneously reproduce the luminosity functions observed in the core, at $\sim 3'2$, $4'5$, and $10'$ away from the center, as well as the surface brightness and velocity dispersion profiles of red giant stars only if the model IMF rises as $m^{-1.6 \pm 0.2}$ in the range $0.8 - 0.3 M_\odot$ and then drops as $m^{0.2 \pm 0.1}$ below $\sim 0.3 M_\odot$. Adopting a more physical log-normal distribution for the IMF, all these data taken together imply a best fit distribution with $m_c \simeq 0.3$ and $\sigma \simeq 1.8$.

Subject headings: stars: Hertzsprung–Russel (HR) and C-M diagrams – stars: luminosity function, mass function – Galaxy: globular clusters: individual: NGC 6397

1. Introduction

Among the Galactic globular clusters (GC), NGC 6397 has so far been the preferred target in the quest for the lowest mass stars that could tell us much about the IMF of these systems and clarify whether or not they can hide a substantial fraction of their total mass in the form of very light objects. The close proximity of NGC 6397 (~ 2 kpc) coupled with its low metallicity ($[\text{Fe}/\text{H}] \sim -1.9$; Djorgovski 1993) makes stars at the bottom of the main sequence (MS) relatively easy to observe with the powerful cameras on board the HST, and many have undertaken this challenge. Our original work on this subject (Paresce, De Marchi, & Romanelli 1995) revealed for the first time a marked deficiency of low-mass stars with respect to expectations based on a power-law mass function (MF) increasing all the way to the Hydrogen-burning limit (Fahlman et al. 1989). These findings were questioned by Cool, Piotto, & King 1996 and Chabrier & Méra (1997), but have since been largely confirmed by independent measurements (Mould et al. 1996; King et al. 1998) which all concur to suggest a MF that flattens out below $\sim 0.3 M_{\odot}$. We argue in this paper that below $0.3 M_{\odot}$ the MF drops all the way to the detection limit at the bottom of the stellar MS.

Although the results mentioned above seem to be consistent with each other, and thus rather robust, there are at least two practical issues that need to be carefully addressed. First of all, it is fair to wonder to which extent this deficiency of low-mass stars at the bottom of the MS is physical and genuine and how much of it should rather be attributed to some limitation inherent in the instrument or method of data analysis used. In fact, the observations carried out so far are con-

fined to the optical domain (V and I bands), while low- and very-low mass stars such as those near the H-burning limit are expected to have a spectral energy distribution that peaks in the near-IR at $\sim 1.2 \mu\text{m}$ (Allard & Hauschildt 1995). If a large population of very faint and redder stars were present in this cluster, they might escape detection with the WFPC2. Secondly, the accurate determination of a luminosity function (LF) from these observations requires a reliable assessment of the contamination due to background unresolved galaxies and to field stars which are rather numerous at the low galactic latitude of NGC 6397 ($b_{\text{II}} \simeq -12$). Attempts have been made to account and correct for this contamination using both color and proper motion information, but both methods are subject to some uncertainties.

Finally, a third, more general question needs to be addressed concerning the real meaning of these localized MF, namely whether the observed flattening at low masses is a feature inherent in the global MF (GMF) or, even, in the IMF of the cluster, or whether it simply results from the internal dynamical modification of an originally completely different mass distribution. Although Richer et al. (1991) have proposed that, if measured near the half-mass radius, the present day MF should closely resemble the IMF, no direct confirmation of this hypothesis exists yet.

In this paper, we address all three issues above. The first two are best attacked with the new NICMOS camera on board the HST, which we have used to investigate the stellar population of NGC 6397 precisely at the wavelengths where low mass stars are expected to shine the most, and to sample a control field located well outside of the cluster tidal radius to provide an independent

estimate of field object contamination. We address the third issue by modelling the dynamical state of NGC 6397 in Section 5, where we put together all the LF currently measured for this cluster at various radial distances and compare them with the predictions of a multi-mass model that takes internal dynamical evolution (mass segregation) into account.

2. The Data

The results of this paper are based on observations obtained by us with both the NIC 2 and NIC 3 cameras of the NICMOS instrument on board the HST (MacKenty et al. 1997). NIC 2 was used on 1997, Sep 30 to observe a region located ~ 4.6 NW of the center of NGC 6397 (hereafter field F 2) through the F110W and F160W broad band filters with a total exposure time of 10,235 s and 4,027 s, respectively. The field of view of the NIC 2 camera ($\sim 19'' \times 19''$) was placed over an area previously imaged with the WFPC 2 (see Paresce et al. 1995). A field closer to the cluster center was observed on 1998, June 17 with the NIC 3 camera (during the second “NIC 3 Campaign”), when the $\sim 50'' \times 50''$ FOV was pointed to RA=17:40:54, DEC=−53:42:57 (J2000) corresponding to a distance of 3.2' from the center (hereafter Field F 1) and images were taken for a total exposure duration of 2,303 s in F110W and of 703 s in F160W. In units of the cluster’s half-light radius ($r_{\text{hl}} = 175''$ Djorgovski 1993), our NIC 2 and NIC 3 fields are located, respectively, at $\sim 1.6 r_{\text{hl}}$ and $\sim 1.1 r_{\text{hl}}$. We also used the NIC 3 camera to observe a comparison field (hereafter SKY), located 2° NE of the cluster at RA=17:47:52, DEC=−51:41:17 (J2000), to estimate the contamination due to field stars and correct for it in a statisti-

cal way. The filters and exposure times are identical to those used for the field F 1.

The quality of all these data sets is excellent, with PSF full width at half maximum (FWHM) of $\sim 0''.13$ for NIC 2 and of $\sim 0''.19$ for NIC 3 (achieved through the repositioning of HST’s secondary mirror operated during the NIC 3 campaign). Images were subjected to the standard STSDAS calibration (CALNICA) to remove the instrumental signature (bias and flat field correction) and, in the case of the NIC 2 images, multiple frames of the same area and taken through the same filter were combined to improve the statistics. The average per-pixel count-rate of the background is of order $0.03 \pm 0.015 \text{ count s}^{-1}$ in F110W and $0.02 \pm 0.008 \text{ count s}^{-1}$ in F160W for the NIC 2 data, and $0.11 \pm 0.01 \text{ count s}^{-1}$ in F110W and $0.12 \pm 0.01 \text{ count s}^{-1}$ in F160W for NIC 3 images. These values, and particularly the standard deviation of the background, are larger than those predicted with the NICMOS simulator, but still within a factor of two of them.

The automated star detection routine *daophot.daofind* was applied to the data, with a detection threshold conservatively set at 5σ above the local average background level (the threshold was set to 10σ for the NIC 3 cluster field as it is more crowded than the others, and the severe PSF under-sampling of NIC 3 makes it very difficult to detect and measure faint stars near brighter objects). We carefully examined by eye each individual object detected by daofind and discarded saturated stars, a number of features (PSF tendrils, noise spikes, etc.) that daofind had interpreted as stars, as well as a few extended objects (with FWHM larger than twice that typical of point sources). The number of well defined objects detected in this way amounts

to 517 in the F 1 field, 58 in the F 2 field, and 119 in the SKY comparison field. We should notice here that we have used our knowledge of the quantum efficiency and filter transmission of NICMOS in the F110W and F160W filters (see Pulone et al. 1998) to select exposure times in these bands such that a typical M-type dwarf in NGC 6397 would be detected with a similar SNR in both bands. And indeed, with an exposure time about ~ 3 times longer in F110W than in F160W, all objects detected in one band are normally also visible in the other.

Since crowding is not too severe in any of our images, stellar fluxes were measured using the standard *digiphot.apphot* IRAF aperture photometry routine, following the prescription of the “core aperture photometry” technique described in De Marchi et al. (1993). Instrumental magnitudes were then calibrated and converted into the HST magnitude system (STMAG) following the relation:

$$m_{ST} = -2.5 \log \left(\frac{cU}{\varepsilon t} \right) \quad (1)$$

where c is the number of counts measured for each star, U the inverse sensitivity of the instrumental setup (camera + filters), ε the encircled energy (i.e. the aperture correction), and t the total exposure time. The internal accuracy of our photometry ranges from < 0.05 mag at $m_{160} \simeq 18$ to ~ 0.5 mag at $m_{160} \simeq 26$, although, particularly for the F110W observations taken with NIC3, the highly variable pixel response function of the camera can introduce statistical uncertainty of up to $\sim 10\%$ (Storrs 1998). Due to the current uncertainty affecting the photometric zero points of the NIC3 camera (Nota et al. 1998), our absolute photometry is accurate to within the 5% – 10% level. In order

to make it easier to directly compare our results with those obtained from the ground, we translate our measurements from the STMAG system into the VEGAMAG photometric system of the HST, defined as one in which the magnitude of Vega would be 0 in all bands and which is more similar to the classical Johnson–Cousin ground-based system. We adopt the VEGAMAG system in this paper and do so by subtracting the zero-point constants of 2.3 mag and 3.7 mag from the values of the STMAG magnitudes in the F110W and F160W bands, respectively. In the following, we refer to these magnitudes as to J and H , respectively.

With the magnitudes measured in this way we have produced the color-magnitude diagrams (CMD) shown in Figure 1 (panels a – c). The MS of cluster stars is well defined in the F 1 field (NIC3, Figure 1 a), extending from $H \simeq 14.5$ to $H \simeq 22$ where it broadens due to increasing photometric errors. The MS of the stars in the F 2 field (Figure 1 b) is sparser and less well defined, but it occupies the same region in the CMD as that of the F 1 field. The latter, however, appears consistently broader than the former at any magnitude. This effect is likely to be the result of the non uniformity of the sensitivity across the surface of the pixels of the NIC3 camera (Storrs 1998), coupled with the severe under-sampling of the PSF. The expected ensuing uncertainty in the photometry is larger for the F110W data (of order 11%) than for the F160W filter ($\sim 6\%$), and is in agreement with the observed MS broadening.

The lines in Figure 1 a and 1 b represent the theoretical MS of a 10 Gyr old population with the metallicity and distance appropriate to NGC 6397 as obtained using the models of Baraffe et al. (1997). We have

assumed the metal content $[Fe/H] = -1.9$ and extinction coefficient $E(B - V) = 0.18$ as given by Djorgovski (1993), but have let the distance take on two different values, i.e. $(m - M)_0 = 11.7$ from Djorgovski (1993; solid line in Figure 1) and $(m - M)_0 = 12.2$ from Reid & Gizis (1998; dashed line). The theoretical sequences reproduce very well our observations, and, particularly, the change of slope occurring at $H \simeq 17.5$ and due to the change of the main source of opacity in the atmosphere of the stars from H^- to H_2 . Because of the uncertainty in the zero point of our photometry and of the broadening of the MS due to the intra-pixel sensitivity variation of the NIC3 camera we cannot decide which of the two distance scales is more appropriate, in that they are both consistent with our observations. The mass values printed along the right-hand axes of Figure 1 are derived from the M-L relation of Baraffe et al. (1997) for a distance modulus of $(m - M)_0 = 12.2$ (Reid & Gizis 1998).

Comparing the CMD of the F 1 field with that of the SKY field (Figure 1c) immediately reveals that field stars (mostly disk objects, owing to the low Galactic latitude of NGC 6397, $b_{II} = -12$) occupy exactly the same location in the diagram as the cluster objects. It is thus not possible to assign cluster membership to a star on the basis of its color alone. This is precisely why we have secured observations of the SKY field so as to be able to account in a statistical way for the contamination due to field stars and affecting our LF (see Section 3).

A robust determination of the LF also requires proper correction for the photometric incompleteness due to crowding. We have thus carried out several standard artificial star tests by adding artificial stars with mag-

nitude values covering the whole range spanned by our observations. For fields F 2 and SKY we have generated 10 artificial images per filter adding each time respectively 8 and 20 stars, and have found that more than 90 % of the artificially added objects are recovered at any magnitude level. The limited crowding and our conservative choice of a 5σ detection threshold combine in such a way that artificial stars are always retrieved unless they fall onto another object. In field F 1, however, crowding is more severe. We ran 20 tests per filter adding 40 stars each time and found that 90 % of the artificially added objects are recovered at $H \simeq 19$ but the completeness gradually drops to $\sim 65\%$ at $H \simeq 22$ as shown in Table 1.

To derive the LF of MS stars in the cluster we have counted the number of objects as a function of the H magnitude in the CMD corresponding to fields F 1 and F 2. We have determined in this way the number of stars in each 0.5 mag bin (1-mag bins were used for F 2), which is then multiplied by the incompleteness coefficient. This latter step needs only be performed for stars in field F 1, as the photometric incompleteness is negligible in fields F 2 and SKY, where the Poisson

Table 1: Table 1 – Photometric completeness in the F 1 field

H magnitude	completeness
15	100 %
16	99 %
17	97 %
18	94 %
19	90 %
20	88 %
21	75 %
22	67 %

statistics of the counting process dominates the final uncertainty on the LF. In order to account in a statistical way for field star contamination, we then subtracted from each bin the number of objects measured in the same magnitude bin of the CMD of field SKY (the area covered by SKY is the same as F 1 and seven times larger than F 2). The LF obtained in this way are shown in Figure 2 in a linear scale as a function of the observed H band magnitude.

Although the LF in field F 2 (bottom of Figure 2) spans a narrower magnitude range than that obtained with NIC 3 in F 1 (top histogram) because of saturation of the few bright stars in field F 2, within the experimental errors the two LF agree very well with each other over the common magnitude interval, once properly scaled. Indeed, although the former LF is affected by large uncertainty, its shape is not different from that measured in F 1, with which it agrees well after having been scaled vertically by a factor of ~ 5 to account for the the larger area covered by F 1. Both LF show a peak near $H \simeq 19$ followed by a clear drop all the way down to $H \simeq 22$, where they become statistically consistent with zero. The error bars plotted in Figure 2 reflect the $\pm 1\sigma$ uncertainty obtained by combining the Poisson statistics on the number counts with the statistical uncertainty associated with the background subtraction. We note here, however, that we have associated a 2σ error bar to the bins in which the net number of stars is < 5 , as in these cases the uncertainty can largely exceed the determined value and one might prefer to use a 2σ upper limit instead. Nevertheless, it is noteworthy that the number of stars becomes compatible with being zero at magnitude very close to that expected for the MS

H-burning limit for stars with the metallicity of NGC 6397 (Baraffe et al. 1997).

3. Comparing the Optical to the Infra-Red Data

NGC 6397 is the first globular cluster for which a deep, reliable LF became available from WFPC 2 photometry of MS stars all the way to the bottom of the MS (Paresce et al. 1995). So far, two other independent studies exist with the WFPC 2 that confirm the deficiency of faint stars near the half-light radius of this cluster discovered by Paresce et al. (Cool et al. 1996; King et al. 1998). A direct comparison of those observations, carried out at optical wavelengths, with our new IR data could clarify whether the WFPC 2 is efficient at detecting faint, red dwarfs or whether it has missed a large amount of the very low mass objects that could potentially account for a conspicuous fraction of the total mass of GC.

The first step in this attempt is to compare deep optical (I band) and IR (H band) images of the same area (field F 2), as we do in Figure 3. It is immediately evident that all the objects detected with NICMOS in the H band with a ~ 170 min exposure (left panel) are also present in the ~ 90 min WFPC 2 image through the I band filter (F814W, right panel). The arrow indicates a star with $M_V = 13.8$, $M_I = 12.4$, $M_J = 11.4$, and $M_H = 10.7$ which, using the distance modulus of Reid & Gizis (1998) and the M-L relation of Baraffe et al. (1997) for $[M/H] = -1.5$, translates to a mass of $\lesssim 0.09 M_\odot$, namely that expected for an object close to the H-burning limit in this cluster (Baraffe et al. 1997). Since this object is clearly visible in all bands (V, I, J , and H), it is unlikely that the WFPC 2 has underestimated the number of low-mass stars. In

principle, then, one should expect the two instruments to give the same LF, but since the number of stars common to both NICMOS and WFPC 2 is small, statistical fluctuations might be important.

A second, perhaps better way to reveal any significant difference between the results of NICMOS and the WFPC 2 data is to compare the IR and optical LF to one another. The wavelength difference, however, would require a transformation from one photometric system to the other, which would inevitably introduce uncertainties that we want to avoid. To minimize possible systematic errors, we prefer to compare to one another the theoretical MF that best fit our visible and IR data.

In Figure 4 a we show the LF of field F 1 in units of absolute H -band magnitude M_H , assuming a distance modulus of $m - M = 12.2$ (Reid & Gizis 1998) and $E(B - V) = 0.18$ (Djorgovski 1993). Figure 4 b shows the LF in the I band (F814W) as measured by Paresce et al. (1995) with the WFPC 2, also converted to absolute magnitude units M_I . The LF in the I band does not cover the whole MS, in that it stops at the bright end ~ 2 mag before reaching the turn-off ($M_I \simeq 4$) due to saturation.

Since it is often assumed for simplicity that, even over a wide mass range, the stellar MF is well represented by a power-law distribution of the form $dN/dm = m^{-\alpha}$ (see, however, Scalo 1998 about the large range spanned by α), we initially adopt such a functional form for the theoretical MF.³ The

³Some authors prefer to express the power-law MF in logarithmic units, i.e. $dN/d\log m = m^{-x}$. The two exponents α and x are such that $\alpha = x + 1$, with Salpeter's IMF taking on the value of $\alpha = 2.35$ and $x = 1.35$, respectively. Throughout the rest of the

dashed lines in Figure 4 show the theoretical LF obtained by multiplying a power-law distribution by the derivative of the M-L relation appropriate to NGC 6397 (Baraffe et al. 1997). This M-L relation is adopted here because it is the only one presently available that takes into account all the stellar physics on the problem and that fits very well all available data on the CMD of globular clusters. The inspection of Figure 4 a and 4 b immediately reveals that a single-exponent power-law distribution is not a viable choice for the underlying MF at this position, regardless of the value of α . And indeed, while the bright portion of the LF up to the peak at $M_H \simeq 6$, $M_I \simeq 8$ requires $\alpha \simeq 1.4$ (acceptable fits are found for $0.8 < \alpha < 1.6$ in the H band, and $1.2 < \alpha < 1.6$ in the I band), a much shallower exponent $\alpha \simeq -0.4$ ($-0.8 < \alpha < -0.4$ in H , $-0.5 < \alpha < -0.1$ in I) is needed to fit the dropping portion of the LF beyond the peak. At the same time, Figure 4 shows that the same type of MF applies to both the optical and IR data, i.e. one that flattens out and drops at $\sim 0.3 M_\odot$, close to the peak of the LF when adopting the M-L relation of Baraffe et al. with the distance modulus and reddening values given above. In other words, the peak and turn over observed in all the LF measured so far for NGC 6397 near the half-mass radius (Paresce et al. 1995, De Marchi & Paresce 1997, King et al. 1998) cannot be attributed exclusively to the change of slope of the M-L relation at $\sim 0.3 M_\odot$.

This result is fully consistent with the conclusions of Paresce et al. (1995) and De Marchi & Paresce (1997), showing that they apply to the IR as well. *We can, there-*

paper we will use the linear notation (α), except for Figure 6 which, as we explain, is best displayed in logarithmic units.

fore, exclude that near the half-light radius of NGC 6397 the MF of the stellar population is represented by a single-exponent power-law distribution as advocated by Chabrier & Méra (1997) and Silvestri et al. (1998). Chabrier & Méra (1997) reach this conclusion by assuming that the last four bins of Paresce et al. (1995) can be safely ignored as being seriously affected by incompleteness. This is now known not to be the case. Silvestri et al. (1998) reach this conclusion by using a model that is inconsistent with the observed CMD of NGC 6397 and other clusters. This is most likely due to their use of a grey-like atmosphere approximation which Chabrier & Baraffe (1997) have convincingly demonstrated to be wrong below $\sim 0.6 M_{\odot}$.

4. Local Mass Function or Global Mass Function ?

It is well known that, through the relaxation process, stars in GC tend to reach energy equipartition and, as a result, their mass spectrum can vary in time and space (Spitzer 1987) so that, for instance, the MF measured in the core of a cluster in thermal equilibrium should decrease with decreasing luminosity. Paresce, De Marchi, & Jedrzejewski (1995), King, Sosin, & Cool (1995), and De Marchi & Paresce (1996) have indeed shown this to be precisely the case, in the mass range $0.8 - 0.5 M_{\odot}$, respectively for 47 Tuc, NGC 6397, and M 15. At this juncture, it is fair to wonder whether the flattening below $\sim 0.3 M_{\odot}$ that we now observe in the MF of field F 1 and F 2 is an intrinsic feature of the IMF, or perhaps a characteristic signature of the global MF, or whether it simply is the result of some local dynamical effects bearing no relation whatsoever with either the IMF or the global MF. Although conventional wis-

dom and theoretical models suggest that away from both the cluster center and from its periphery these effects should be rather modest (Richer et al. 1991; Vesperini & Heggie 1997), no unambiguous proof exists that this hypothesis is correct, nor does one exactly know where (if anywhere) the local MF should be most insensitive to dynamical modifications. Thus, since NGC 6397 is probably in an advanced evolutionary state and has probably already gone through the collapse phase, the two-body relaxation process that has strongly changed the properties of the stellar population in the cluster's core (King et al. 1995) might have worked its effects farther out in the periphery, possibly imparting non negligible modifications onto the MF in the regions that we observed. And indeed, a careful inspection of Figure 4 already reveals that, although similar, the MF that best fits the LF in field F 1 is not precisely the same that one requires to properly reproduce the LF observed in field F 2 (see discussion above).

In an attempt to clarify this issue and to put more stringent constraints on the shape of the cluster's global MF (and, possibly, on its IMF), we have computed the effect of the segregation mechanism in NGC 6397 by using a dynamical model of the cluster so that we could compare our observations with the predicted shapes of the LF at several radial positions. Besides the data obtained in field F 1 ($r \simeq 3.2'$) with NIC3 and in field F 2 ($r \simeq 4.5'$) with WFPC2 and NIC2, we have included in this exercise the data taken with the WFPC2 by Mould et al. (1996) in a field located $\sim 10' N$ of the cluster center. In order to ensure that the comparison of these latter data to our own observations is not hampered by possible differences in the way they were reduced, we have extracted from

the HST archive the images taken by Mould et al. (1996) and have subjected them to the same, homogeneous data processing that we have applied to our WFPC2 observations of NGC 6397 (Paresce et al. 1995).

Observations of Mould et al.'s field (hereafter called F 3) are available through both the F555W and F814W bands, with a total exposure time of 3,600 s in each filter. This has allowed us to build a CMD in all ways similar to that of Mould et al. (see their Figure 1), to which we have applied our “ 2.5σ -clipping” criterion to discriminate, in a statistical way, the stars belonging to the cluster from field objects (see De Marchi & Paresce 1995 for a detailed description of the method). The LF of MS stars determined in this way agrees reasonably well with that measured by Mould et al., in that both LF increase with decreasing luminosity up to a peak at $m_{814} \simeq 20.5$ and then fall off. Theirs, however, reveals a secondary peak at $m_{814} \simeq 22$ ($M_I \simeq 9.5$) that we do not see and which is most likely the result of a different amount of correction for field star contamination. We would like to point out that the latter represents the largest source of uncertainty in the determination of the LF in field F 3, and that this effect is much more severe than that made by ignoring the photometric incompleteness as both Mould et al. and we have done. The resulting LF is shown in Figure 5 after having been converted into units of absolute magnitude by adopting the distance modulus given above.

5. Modelling Mass Segregation

We have employed the multi-mass Michie-King models developed by Meylan (1987, 1988), and which were later adopted by Meylan & Mayor (1991) to study the dynamical proper-

ties of NGC 6397. Each model is characterized by an IMF in the form of an exponential $dN/dm = m^{-\alpha}$, with a variable exponent α , and by four structural parameters describing respectively the scale radius (r_c), the scale velocity (v_s), the central value of the dimensionless gravitational potential W_o , and the anisotropy radius (r_a). From the parameter space defined in this way, Meylan & Mayor (1991) have selected those models that simultaneously fit both the observed surface brightness (SBP) and velocity dispersion (VDP) profiles of the cluster. The fit to the SBP and VDP, however, can only constrain r_c , v_s , W_o , and r_a while still allowing the IMF to take on a variety of shapes. To break this degeneracy, we have complemented Meylan's code by imposing the condition that the model MF agree with the observed LF, following precisely the approach that we used in our investigation of the globular cluster M 4 (Pulone, De Marchi, & Paresce 1999).

As we explain in that paper, Michie-King modeling only provides a “snapshot” of the current dynamical state of the cluster. It is, then, useful to define the global mass function (GMF), i.e. the mass distribution of all cluster stars at present, as the MF that the cluster would have simply as a result of stellar evolution (i.e. ignoring any local modifications induced by internal dynamics and/or the interaction with the Galactic tidal field). Clearly, in this case the IMF and GMF of MS (un-evolved) stars is the same. For practical purposes, the GMF has been divided into sixteen different mass classes, covering MS stars, white dwarfs, and heavy remnants, precisely as described in Pulone et al. (1999).

The SBP and VDP used in our simulations are taken from the paper of Meylan & Mayor (1991), as G. Meylan kindly gave us the data

in electronic form. Since these authors provide the mass, density, and structural parameters of the 8 models that best reproduce the observed radial profiles (SBP and VDP), we have tested whether the predicted LF would also agree with our observations. Our exercise confirms what we have already shown in Figure 4: as long as a single value of the exponent α is used for the IMF over the mass range $0.1 - 0.8 M_{\odot}$, none of these 8 models gives local MF that, converted into LF using the M-L relation described above, agree with our data. In fact, if the exponent α is selected in such a way that the rising portion of the LF is well fitted (this requires $\alpha \simeq 1.6$), the model LF consistently deviate from the observations beyond the peak at $M_I \simeq 8.5$, $M_H \simeq 6.5$ because they fall off too slowly. Similarly, to fit the falling portion of the LF one would require $\alpha \simeq -0.2$, which would in turn overestimate the number of bright stars.

On the other hand, if the model IMF is allowed to flatten out below $\sim 0.3 M_{\odot}$, both portions of the three observed LF can simultaneously be fitted while, at the same time, the SBP and VDP are adequately reproduced. In particular, we find that an exponential IMF with index $\alpha = 2 \pm 0.2$ for evolved stars ($m > 0.8 M_{\odot}$), $\alpha = 1.6 \pm 0.2$ in the range $0.8 - 0.3 M_{\odot}$ and which drops with $\alpha = -0.2 \pm 0.1$ at lower masses would not only produce a good fit to the LF observed in field F 1, F 2, and F 3 (Figure 5), but would also give reasonable values for the cluster's structural parameters: the concentration ratio ($c \simeq 2.6$), the total cluster mass ($\simeq 8.9 \times 10^4 M_{\odot}$), the fraction of heavy remnants ($\sim 33\%$ in mass, about half of which in the form of neutron stars of $1.2 M_{\odot}$ and the rest in the form of heavy white dwarfs of $0.6 M_{\odot}$), and the anisotropy radius ($r_a/r_c \simeq 20$) are all in excel-

lent agreement with those of the 8 best models of Meylan & Mayor (1991).

King et al. (1998) notice that the somewhat large value of the core radius that Meylan & Mayor (1991) obtain (and that we only marginally decrease here) does not allow them to accurately reproduce the SBP in the innermost regions of the cluster. On the other hand, Meylan & Mayor point out that the deviation of the observed profile from that of a typical Michie-King model in the central regions is most likely the result of random fluctuations due to a few bright stars, whose distribution is not uniform (Aurière, Lauzeral, & Ortolani 1990). Moreover, if the core of NGC 6397 has already been through its collapse phase, a classical King-type profile (King 1962) of a cluster in equilibrium certainly does not provide the most appropriate representation of the SBP and the value of r_c that one would deduce from it would be rather uncertain.

To test whether our model also gives a proper account of the properties of the stellar population in the core, we have compared the MF that it predicts at $\sim 7''$ from the center with that measured by King et al. (1995) with the FOC on board HST. Although our model seems to predict a somewhat slower decline than that reported by King et al. in the range $0.7 - 0.4 M_{\odot}$ (namely $\alpha \simeq -2$ vs. their $\alpha \simeq -2.7$), this discrepancy should not be taken too seriously in view of the limitations of our model and of the uncertainties that could affect the conversion of the observed LF from the F480LP band of the FOC into the Johnson's V band, and then from that into the F814W band of the WFPC 2 and, finally, into a MF by the use of a rather crude M-L relation. We can, therefore, conclude that the two MF are in fairly reasonable agreement

with each other, in that they both indicate an inverted function (i.e. stars are decreasing with decreasing mass) starting already at the turn-off.

6. Discussion

The result stemming from Figure 5 and from the discussion above is fully consistent with our findings in Section 3. *Not only can we exclude that the local MF measured near the half-light radius come from a single exponent power-law, but we also prove here that not even the global MF from which they originated through energy equipartition can be a function of that type.* These findings carry the important implication that, if NGC 6397 has not experienced too strong an interaction with the Galactic tidal field or bulge (but see Gnedin & Ostriker 1997), also the IMF has to flatten out and, possibly, drop below $\sim 0.3 M_{\odot}$.

Since, however, Nature has always shown a predilection for smooth variations, it might seem rather unphysical that the IMF or GMF of MS stars can have such an abrupt change of slope at $\sim 0.3 M_{\odot}$ as our work seems to imply. Clearly, our fit to the GMF is nothing but a mathematical over-simplification, dictated by the adoption of a power-law as representative of the distribution of stellar masses. As Scalo (1998) points out, this assumption might be correct for intermediate mass stars, but fails at the edges of the distribution (very low and very high masses). Although we could have used more than two values of the exponent α to fit the change of slope, that would have appeared as an unwarranted sophistication whose physical meaning remains uncertain. Thus, since the most important implication of Figures 4 and 5 is that the MF of NGC 6397 cannot be reproduced

using a single exponent power-law distribution, one wonders why choosing two or more power-laws would make any sense at all.

There is, however, a large amount of theoretical work suggesting that the star formation process would preferentially give rise to a mass distribution that deviates from a pure power-law. Zinnecker (1984) and, more recently, Adams & Fatuzzo (1996) have pointed out that, if the number of parameters governing the fragmentation process of protostellar clouds is sufficiently large (of order 5 or more), the central-limit theorem immediately implies that the IMF should take on a log-normal form. A similar IMF is obtained independently by Elmegreen (1997, 1999) with a different theoretical approach. If we adopt the formalism of Adams & Fatuzzo (1996), the IMF is characterized by two parameters, namely the characteristic mass m_c and the standard deviation σ and takes on the form:

$$\ln f(\log m) = A - \frac{[\log(m/m_c)]^2}{2\sigma^2} \quad (2)$$

where A is a normalization constant. The Miller & Scalo (1979) IMF (now superseded; Scalo 1998) would require $m_c \simeq 0.095 M_{\odot}$ and $\sigma = 1.57$, while the Scalo (1986) IMF (now also extinct; Scalo 1998) would imply both a larger value of m_c and a smaller width σ . In Figure 6 we show that, within the observational uncertainties, the GMF of NGC 6397 is consistent with a log-normal distribution having $m_c \simeq 0.3 M_{\odot}$ and $\sigma \simeq 1.8$. Interestingly, these values are very similar to those found for MS stars in the Pleiades (Bouvier et al. 1998).

7. Summary and Conclusion

The main results of this paper can be summarized as follows:

- The properties of the stellar population of NGC 6397 as determined with deep IR observations obtained with NICMOS on board the HST are fully consistent with those stemming from similarly deep WFPC2 optical data. In particular, down to the bottom of the cluster's MS, NICMOS does not show any more faint, red objects than those already detected by the WFPC2, thus confirming that there are no stars contributing significantly to the low-mass budget of the cluster which can be detected in the IR and not in the I band. Thus, the unavailability of NICMOS will not hinder this investigation in the future.
- A comparison of our deep IR CMD with the theoretical models of Baraffe et al. (1997) shows the agreement to be excellent, thus proving that the latter are reliable also in the IR domain.
- The IR LF of MS stars near the cluster's half-light radius, measured using a comparison field located a few degrees away from the cluster center to correct for the contamination due to foreground and background objects, is fully consistent with those obtained with the WFPC2 in the I band using different and independent techniques to separate cluster members from field stars, namely the color selection of Paresce et al. (1995) and the proper motion study of King et al. (1998).
- Using the M-L relations of Baraffe et al. (1997), all three LF translate into

MF in which the number of objects per unit mass increases exponentially as $\sim m^{-1.5}$ in the range $0.7 - 0.3 M_{\odot}$ and then flattens out and drops. We show that a simple power-law distribution of the form $m^{-\alpha}$ cannot reproduce any of these LF if the exponent α is kept constant, regardless of its value.

- The relaxation mechanism and the ensuing mass segregation process inside the cluster is studied under the assumption that a simple isothermal model of a cluster in equilibrium is a viable choice for NGC 6397 and ignoring the effects of tidal stripping due to the Galaxy, as they do not seem to play any significant role in reshaping the MF of this cluster (Paresce & De Marchi 1999). The model can accurately and simultaneously reproduce the LF observed in regions located $\sim 3'2$, $4'5$, and $10'$ away from the center, the inverted LF in the core, as well as the SBP and VDP of red giant stars only if the IMF rises as $m^{-1.6 \pm 0.2}$ in the range $0.8 - 0.3 M_{\odot}$ and then drops as $m^{0.2 \pm 0.1}$ below $\sim 0.3 M_{\odot}$. The error bands associated with the quoted exponents assume that the M-L relations of Baraffe et al. (1997) are not affected by statistical uncertainties.
- The IMF that we obtain is fully consistent with a log-normal distribution peaked at $m_c \simeq 0.3 M_{\odot}$ and with standard deviation $\sigma \simeq 1.8$.

In this paper we show that a robust and reliable determination of the IMF of GC requires the effects of dynamical evolution to be taken into proper account. Although we have used the best LF currently available for

NGC 6397, we are still forced to rely on uncertain brightness and velocity dispersion radial profiles and on very simple Michie–King multi-mass quasi-equilibrium models to convert a locally determined present day mass function into a global MF. In fact, while the models that we have used are currently the state of the art, they work only under the strict condition that the cluster be fully relaxed and in dynamical equilibrium. Episodes of core collapse and, especially, gravitational shocking due to repeated interactions with the bulge and disk of the Galaxy, however, may profoundly disrupt this distribution by ejecting low mass stars from the core and by compressing the tidal boundary in phase space at each encounter (see e.g. De Marchi et al. 1999). Until these effects can properly be accounted for in future models of this sort, we should obtain the global cluster MF directly by observation through a systematic, precise, and complete census of the entire stellar population of GC spanning a wide range of possible evolutionary scenarios. Specifically, one needs to determine the exact shape of the cluster LF at many locations in the cluster from the main sequence turn-off down to at least the peak of the LF at $\sim 0.3 M_{\odot}$. These local LF and the resulting global MF can then be compared to the available cluster models to assess their validity under differing circumstances. This project is within easy reach of a large telescope such as the VLT.

We would like to thank Georges Meylan for providing us with the original code of his dynamical model and Isabelle Baraffe and Gilles Chabrier for many useful discussions. We are indebted to Haldan Cohn, the referee of this work, for his invaluable comments that have considerably strengthened our paper.

REFERENCES

Adams, F., and Fatuzzo, M. 1996, *ApJ*, 464, 256

Allard, F., and Hauschildt, P 1995, *ApJ*, 445, 433

Auerière, M., Lauzeral, C., and Ortolani, S. 1990, *Nature*, 344, 638

Baraffe, I., Chabrier, G., Allard, F., & Hauschildt, P. 1997, *A&A*, 327, 1054

Bouvier, J., Stauffer, J., Martin, E., Barrado y Navascues, D., Wallace, B., and Bejar, V. 1998, *A&A*, 336, 490

Chabrier, G., & Baraffe, I. 1997, *A&A*, 327, 1039

Chabrier, G., & Méra, D. 1997, *A&A*, 328, 83

Cool, A., Piotto, G., & King, I. 1996, *ApJ*, 468, 655

De Marchi, G., Leibundgut, B., Paresce, F., and Pulone, L. 1999, *A&A*, 343, L9

De Marchi, G., Nota, A., Leitherer, C., Ragazzoni, R., & Barbieri, C. 1993, *ApJ*, 419, 658

De Marchi, G., & Paresce, F. 1995, *A&A*, 304, 202

De Marchi, G., & Paresce, F. 1996, *ApJ*, 467, 658

De Marchi, G., & Paresce, F. 1997, *ApJ*, 476, L19

Djorgovski, S. 1993, in *ASP Conf. Ser.* 50, *Structure and Dynamics of Globular Clusters*, ed. S. Djorgovski & G. Meylan (San Francisco: ASP), 273

Elmegreen, B. 1997, *ApJ*, 486, 944

Elmegreen, B. 1999, *ApJ*, 515, 323

Gnedin, O., and Ostriker, J. 1997, *ApJ*, 474, 233

King, I. 1962, AJ, 67, 471

King, I., Anderson, J., Cool, A., and Piotto, G. 1998, ApJ, 495, 796

King, I.R., Sosin, C., and Cool, A. 1995, ApJ, 452, L33

MacKenty, J. et al. 1997, NICMOS Instrument Handbook, Version 2.0, (Baltimore: STScI)

Meylan, G. 1987, A&A, 184, 144

Meylan, G. 1988, A&A, 203, 297

Meylan, G. and Mayor, M. 1991, A&A, 250, 113

Miller, G., and Scalo, J., 1979, ApJS, 41, 513

Mould, J., et al. 1996, PASP, 108, 682

Nota, A., et al. 1998, NICMOS Photometry Update, (Baltimore: STScI)

Paresce, F., & De Marchi, G. 1999, ApJ, submitted Jun 9

Paresce, F., De Marchi, G., and Jedrzejewski, R. 1995, ApJ, 442, L57

Paresce, F., De Marchi, G., & Romaniello, M. 1995, ApJ, 440, 216

Pulone, L., De Marchi, G., and Paresce, F. 1999, A&A, 342, 440

Pulone, L., De Marchi, G., Paresce, F., & Alard, F. 1998, ApJ, 492, L41

Reid, N., and Gizis, J. 1998, AJ, 116, 2929

Richer, H., Fahlman, G., Buonanno, R., Fusi Pecci, F., Searle, I., & Thompson I. 1991, ApJ, 381, 147

Scalo, J. 1986, Fund. Cosm. Phys., 11, 1

Scalo, J. 1998, in ASP Conf. Ser. 142, The Initial Mass Function, Eds. G. Gilmore and D. Howell, (San Francisco: ASP), 201

Silvestri, F., Ventura, P., D'Antona, F., and Mazzitelli, I. 1998, ApJ, 509, 192

Spizer, L. 1987, Dynamical Evolution of Globular Clusters, (Princeton: PUP)

Storrs, A. 1998, Instrument Science Report NICMOS-98-006, (Baltimore: STScI)

Vesperini, E., and Heggie, D. 1997, MNRAS, 289, 898

Zinnecker, H. 1983, MNRAS, 210, 43

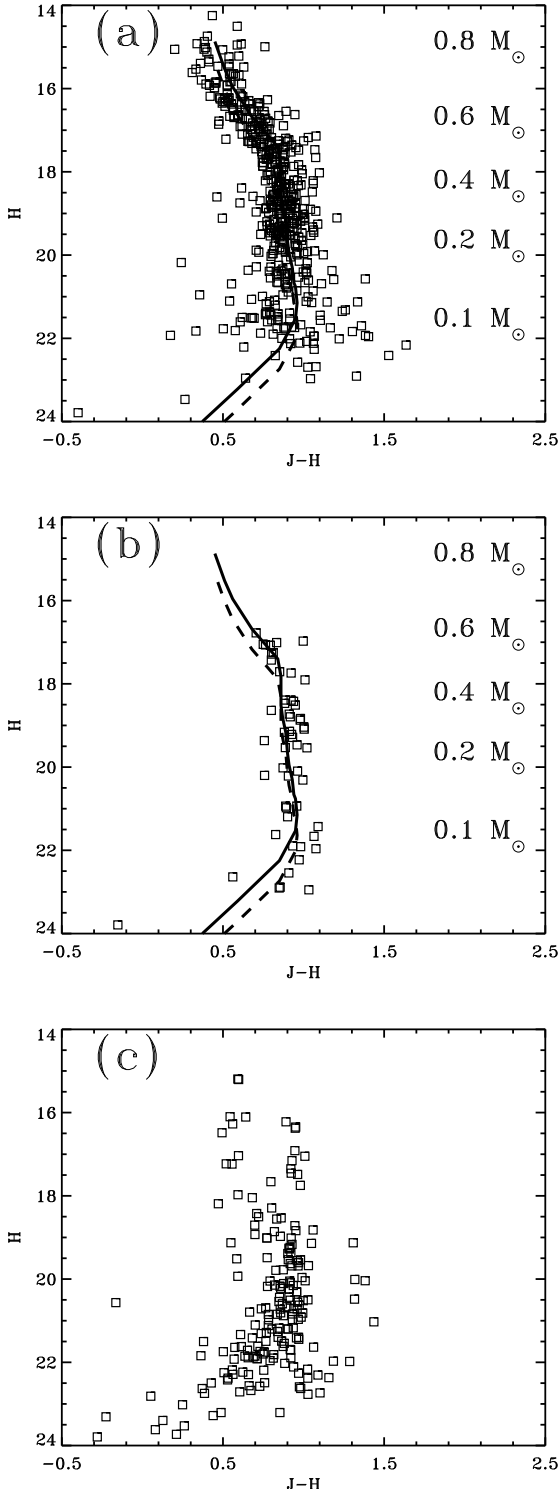


Fig. 1.— IR Color-magnitude diagrams as measured in field F1 (a), F 2 (b), and SKY (c). The magnitudes are given in the VEGAMAG system. See the text for an explanation of the lines in panel (a) and (b).

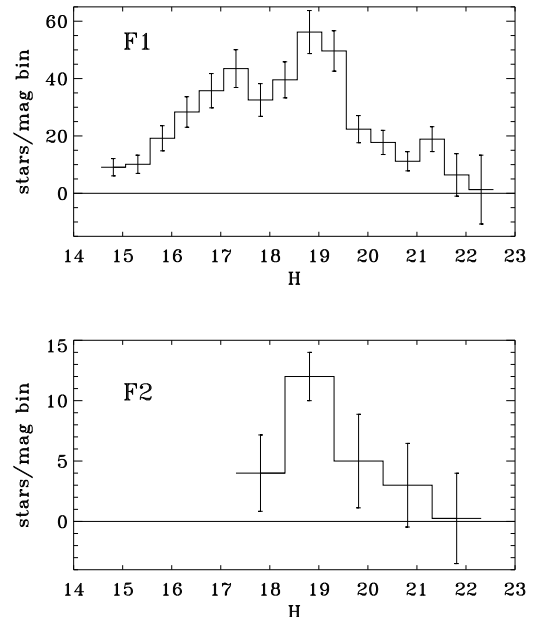


Fig. 2.— IR luminosity functions as measured in field F 1 (top histogram) and F 2 (bottom histogram). Error bars reflect the $\pm 1\sigma$ uncertainty of the Poisson statistics on the number counts and the statistical uncertainty associated with the background subtraction. Note, however, that we have associated a 2σ error bar to the bins in which the net number of stars is < 5 , as in these cases the uncertainty can largely exceed the determined value and one might prefer to use a 2σ upper limit instead.

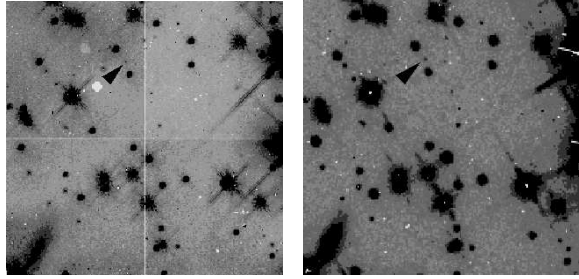


Fig. 3.— Comparison of the same area (field F2) as seen in a with NICMOS NIC2 in the H band with a ~ 170 min exposure (left panel) and in a ~ 90 min duration WFPC2 image through the I band filter (F814W, right panel). The arrow indicates a star close to the H-burning limit in this cluster (see text).

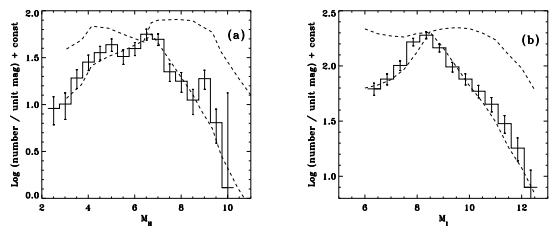


Fig. 4.— Comparison between the IR and optical LF: (a) LF of stars in field F1 in units of absolute H -band magnitude M_H , and (b) the LF in the I band (F814W) as measured by Paresce et al. (1995) with the WFPC2, also converted to absolute magnitude units M_I . The dashed lines show the best fitting underlying MF, characterized by $\alpha = 1.2$ and $\alpha = -0.6$ respectively for the rising and dropping portion of the H band LF, and $\alpha = 1.4$ and $\alpha = -0.3$ in the I band. Acceptable fits are obtained for α within about ± 0.2 of the best fitting values, as explained in the text.

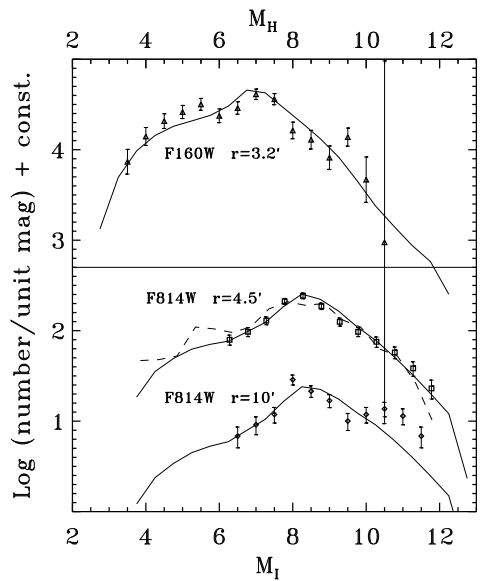


Fig. 5.— The solid lines show the LF predicted by the dynamical model that best fits simultaneously the data at $3.2'$ (triangles), $4.5'$ (boxes), and $10'$ (diamonds) radial distance as well as the SBP and VDP (see text). The scale on the top axis refers only to the IR LF at $r = 3.2$. The dashed line shows the LF as measured by King et al. (1998) in a different region of the cluster, yet still $\sim 4.5'$ away from the center.

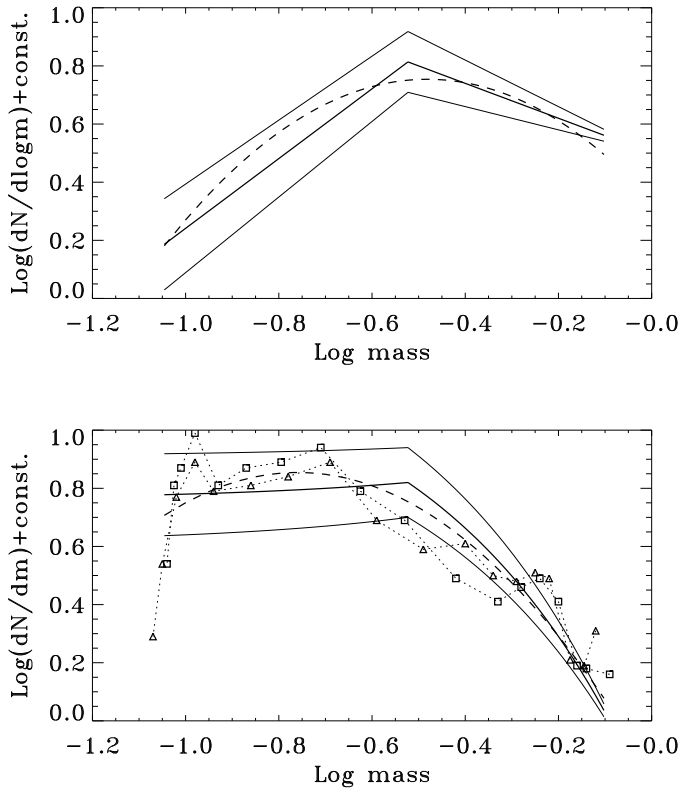


Fig. 6.— Top panel: The GMF of NGC 6397 as predicted by our dynamical model (thick solid line) is consistent, within the error band marked by the thin lines, with a log-normal distribution having $m_c \simeq 0.3 M_\odot$ and $\sigma \simeq 1.8$ (dashed line). The error band corresponds to the uncertainty in the slopes of the two power-law segments used to represent the IMF in our dynamical model (see Sections 3 and 5) and, as such, it does not directly reflect the statistical fluctuations of each individual bin in our LF. Please note that, because the log-normal distribution is best represented in units of logarithmic mass, also the power-law curves in the figure are plotted in the same units, i.e. $dN/d\log m = m^{-x}$. The exponent α used throughout the text obeys the relation $\alpha = x + 1$ as explained in Section 3. Bottom panel: Same GMF as above, but in linear mass units, i.e. dN/dm . The dotted lines represent the MF of NGC 6397 as obtained by King et al. (1998) using the mass-luminosity relations of Baraffe et al. (1997), respectively for a distance modulus of 12.05 (boxes) and 12.05 (triangles). See King et al. (1998) for the details.